

Instrument for fine control of drop-on-demand electrohydrodynamic jet printing by current measurement

Cite as: Rev. Sci. Instrum. **90**, 115001 (2019); <https://doi.org/10.1063/1.5090415>

Submitted: 27 January 2019 . Accepted: 15 October 2019 . Published Online: 01 November 2019

Kai Li, Dazhi Wang , Shanshan Yi, Haoran Jia, Jianghong Qian, Zhiyuan Du, Tongqun Ren, Junsheng Liang, Sergio O. Martinez-Chapa , and Marc Madou



[View Online](#)



[Export Citation](#)



[CrossMark](#)

ARTICLES YOU MAY BE INTERESTED IN

[Low current heaterless hollow cathode neutralizer for plasma propulsion—Development overview](#)

[Review of Scientific Instruments](#) **90**, 113303 (2019); <https://doi.org/10.1063/1.5097599>

[The upgraded Polaris powder diffractometer at the ISIS neutron source](#)

[Review of Scientific Instruments](#) **90**, 115101 (2019); <https://doi.org/10.1063/1.5099568>

[Single-pass non-destructive electronic detection of charged particles](#)

[Review of Scientific Instruments](#) **90**, 113301 (2019); <https://doi.org/10.1063/1.5110988>

Lock-in Amplifiers
... and more, from DC to 600 MHz



Instrument for fine control of drop-on-demand electrohydrodynamic jet printing by current measurement

Cite as: Rev. Sci. Instrum. 90, 115001 (2019); doi: 10.1063/1.5090415

Submitted: 27 January 2019 • Accepted: 15 October 2019 •

Published Online: 1 November 2019



Kai Li,¹ Dazhi Wang,^{1,2,a)} Shanshan Yi,¹ Haoran Jia,¹ Jianghong Qian,¹ Zhiyuan Du,¹ Tongqun Ren,^{1,2} Junsheng Liang,^{1,2} Sergio O. Martinez-Chapa,³ and Marc Madou⁴

AFFILIATIONS

¹Key Laboratory for Micro/Nano Technology and System of Liaoning Province, Dalian University of Technology, Dalian 116024, China

²Key Laboratory for Precision and Non-traditional Machining Technology of Ministry of Education, Dalian University of Technology, Dalian 116024, China

³School of Engineering and Sciences, Tecnológico de Monterrey, Nuevo León, P.C. 64700, Mexico

⁴Department of Biomedical Engineering, Department of Mechanical and Aerospace Engineering, University of California Irvine, Irvine, California 92697, USA

^{a)}Author to whom correspondence should be addressed: d.wang@dlut.edu.cn. Tel.: +86(411)84707170-2171.
Fax: +86(411)84707940.

ABSTRACT

In this work, an instrument of drop-on-demand electrohydrodynamic jet (DoD E-Jet) printing device equipped with a current measurement and control system was designed and developed for finely controlling the printing process. The relationships between the current and printing parameters of voltage, frequency, and flow rate were deeply investigated, and the examination data and conclusion were obtained under the condition of the needle size remaining unchanged. Especially, the equation relationship between the flow rate and current was established, which can be used for the modification of the DoD E-Jet printing process. The map describing the stable printing range, droplet size, and current was also recognized, which can help us to select parameters for stable printing. Based on the current measurement and control system and the established relationship, the optimized current and printing parameters were chosen to print uniform graphene microstructures. This instrument provides an effective method for monitoring, adjusting, and controlling the DoD E-Jet printing process and further improving the quality of the printed structures for micro/nanoelectromechanical system (M/NEMS) devices.

Published under license by AIP Publishing. <https://doi.org/10.1063/1.5090415>

I. INTRODUCTION

Micro/nanostructures have been extensively investigated for high-performance devices in many applications, such as sensors, electronics, and biotechnology.^{1–4} The outstanding properties of high sensitivity, large surface-to-volume ratio, and low power consumption with wide applications are driving the push for improving the micro/nanomanufacturing technology.^{5–8} Printing technique is becoming a powerful method for micro/nanostructure fabrication owing to its purely additive fabrication and no need of mask.^{9–12} Among the emerging printing methods, electrohydrodynamic jet

(E-Jet) printing is a high-resolution direct writing technique that uses an electric field creating the flow of material and enables the printing of micro/nanofeatures.^{13,14} Especially for drop-on-demand (DoD) E-Jet printing, it is a more flexible way to fabricate high-performance devices.^{15–17} During the DoD E-Jet printing process, the stability and consistency of droplets greatly affect the printed structures.¹⁸ However, this process involves many operating parameters, including the applied voltage, pulse frequency, flow rate, and so on. These parameters make the control of this process much more complicated. In order to accurately control DoD E-Jet printing, it is important to establish a monitoring and controlling method to

obtain stable and uniform droplets for fabricating accurate structures.^{19,20} Presently, a microscopy imaging system was usually used to identify the printing status.^{21–25} The optical machine vision system was used for detecting the droplet and filament size.^{26–28} In order to provide detailed information of droplet and jetting behavior, an additional image processing algorithm has to be used for processing the images obtained from the microscopy imaging system. The meniscus image processing method was used to provide the meniscus shape as a feedback signal.²⁹ The imaging device and current detection module were combined to monitor the real-time E-Jet printing process.^{30,31} A closed-loop model predictive control (MPC) feedback module was developed to online regulate the jet diameters near the apex of the Taylor cone.^{32,33} However, these feedback methods were mainly based on visual observation systems, which is difficult to achieve real-time control during the printing process.

In fact, there is a strong relationship between the current, droplet size, and printing parameters. When the voltage is applied between the needle and substrate, electric shearing force is generated and drives the ink to form micro/nanodroplets. During this process, the charges accumulate on the ink surface and move directionally along with the jet and droplets and then the current is generated with the movement of jet and droplets. The relationship between current, flow rate, and ink properties in the spraying mode was investigated.³⁴ A general scaling law that the emitted current has a proportional relationship with the square or four root of the flow rate of the ink in the cone-jet mode was set up.³⁵

In this work, an instrument of fine control of DoD E-Jet printing by the current measurement was designed and established. A DoD E-Jet printing device equipped with a real-time current measurement and control system was developed. The relationships between the current, droplet size, and printing parameters were established. Based on this equipment, the current characteristics

were studied in different printing modes. Then, these relationships were investigated during the DoD E-Jet printing process. The current scaling law in the microdripping mode was analyzed. Moreover, the optimal current range for the condition of stable printing and uniform droplet forming was recognized. Finally, uniform graphene microscale patterns were finely produced using the E-Jet DoD printing under the help of the real-time monitoring and controlling process. This instrument provides a powerful way to finely control the E-Jet DoD printing process and affords a technique for accurate printing microstructures for micro/nanoelectromechanical system (M/NEMS) devices.

II. EXPERIMENTAL AND DESIGN DETAILS

The instrument of fine control of DoD E-Jet printing by the current measurement is illustrated in Fig. 1, which is the printing equipment equipped with a real-time current measurement and control system. As shown in Figs. 1(a) and 1(b), the printing system mainly consisted of a metallic needle, a syringe pump (Harvard Apparatus, Holliston, USA), a waveform generator (Agilent Technologies, USA), a high voltage amplifier (Smart Material GmbH, Germany), an X-Y-Z movement stage (Zolix Instruments, China), and a high speed camera (Fastcam SA4, Photron). In this work, a metallic needle with an inner/outer diameter of 60 μm /160 μm was used for printing, and the data and conclusion were obtained under the condition of the needle size remaining unchanged. The needle inlet was connected to the syringe pump through a silicone tube to feed graphene ink. The high voltage amplifier combined with the waveform generator provided a pulsed electric field between the metallic needle and the aluminum platform. The silicon substrate was placed on the aluminum platform, and it could be moved with the X-Y motion stage. Silver paste was used to connect the silicon

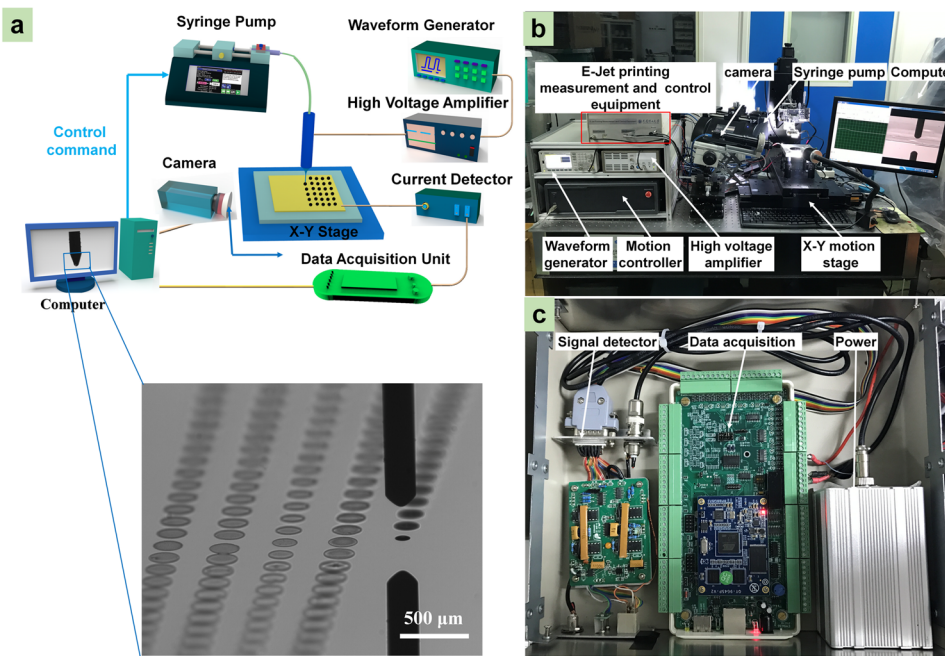


FIG. 1. (a) Schematic of DoD E-Jet printing equipped with the current control system, (b) its equipment setup, and (c) the current measurement and control unit.

TABLE I. Properties of graphene dispersion.

Density (ρ) (kg m $^{-3}$)	Viscosity (μ) (Pa s)	Surface tension (σ) (N m $^{-1}$)	Conductivity (K) (S m $^{-1}$)
9.375×10^2	1.04×10^{-2}	3×10^{-2}	2.52×10^2

substrate and aluminum platform. During the current measuring process in printing, the current detector connected with the aluminum platform. The high speed camera was used for monitoring the printing process in real-time.

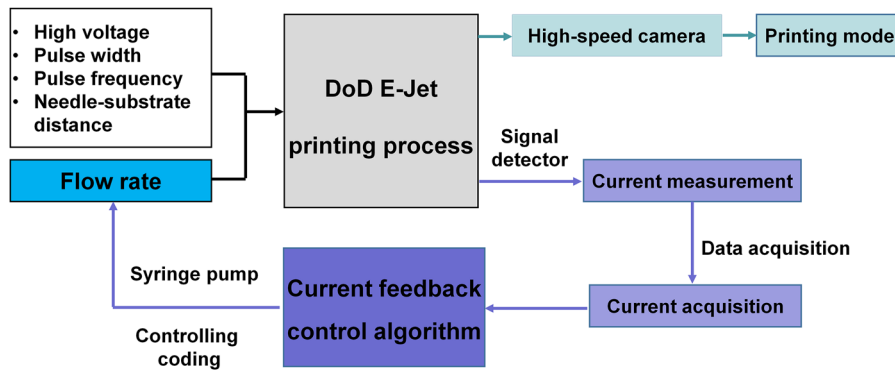
The current measurement and control system composed of a power supply, a current signal detector, and a data acquisition unit. As shown in Fig. 1(c), the power supply was used to supply a direct voltage (20 V) to the signal detector and data acquisition. The signal detector (HB-873, Nanjing University Weak Signal Detection Center) has a current measuring range from 10 pA to 1 mA and a measuring resolution of 10 pA. The data acquisition unit with the maximum sampling frequency of 250 kHz and the maximum throughput of 500 kb s $^{-1}$ communicated with the signal detector and the computer for signal transmission. The current detection process was based on the fundamental physical phenomenon of the DoD E-jet process. When a charged droplet was released from the metallic needle and arrived onto the substrate, the charges can be detected by the signal detector. Then, the data acquisition unit was employed for real-time collecting the current from the signal detector. The detected current data were recoded and uploaded to the computer for controlling the E-Jet printing process. A DoD E-Jet printing program equipped with the current control program was developed based on the LabVIEW software to adjust the flow rate. The syringe pump was connected to the computer through the USB interface. The VISA (Virtual Instrument Software Architecture) module in LabVIEW was used for the communication between the computer and syringe pump. The controlling coding of the flow rate was sent to the syringe pump in the form of SCPI command (Standard Commands for Programmable Instruments). Then, the syringe pump received the controlling command and adjusted the flow rate online.

In this work, graphene dispersion was used for printing structures. Recently, graphene presented the advantages of large specific

surface area, chemical stability, and excellent electrical conductivity, which exhibits promising applications in microelectronics, electrochemical sensors, and energy storage. The graphene dispersion has a solid loading of 2.4 wt. % dispersed in the solvent of ethyl cellulose, cyclohexanone, and terpineol (Sigma-Aldrich). The properties of the graphene dispersion are shown in Table I. Before printing, the substrate was cleaned with acetone, ethanol, and deionized water in sequence. The graphene dispersion was first placed in a 50 μ l glass syringe and delivered to the metallic needle by the syringe pump. Then, an appropriate voltage was applied between the needle and substrate to create an electric field. This electric field induces mobile ions in the graphene dispersion and accumulates near the surface at the tip of the metallic needle. The mutual Coulombic repulsion between the ions introduces a tangential electric field force on the surface of graphene dispersion, along with the electrostatic attraction to the substrate, which deforms the meniscus into a conical shape. Once the electric field force overcame the surface tension of the meniscus, the charged droplets were ejected from the needle and delivered to the target substrate. At the same time, the charges will be transferred to the aluminum platform through the silver paste. Then, these charges will be collected and detected by the current detector. According to the designed patterns and the control of the DoD E-Jet printing program, the substrate was driven by the X-Y-Z motion stage and the DoD E-Jet printing system directly writing the graphene patterns.

In the E-Jet printing process, it takes hundreds of milliseconds for droplets sequentially jetted from the needle and delivered to the target substrate at the frequency of dozens of Hertz; this time is the printing time. In order to obtain more information about this printing process, the “real-time” method of observation, measurement, and control should be smaller at least one order than this printing time. The analysis method at the range of hundreds of microseconds was usually regarded as “real-time” for the E-Jet printing process.^{32,33} According to the above analysis, hundreds of milliseconds are needed for the hemispherical shape ink at the needle tip to get the new balance of surface tension and electric tangential force; this time is called the balance period. In general, the controlling method time smaller than this period can be considered as real-time control in the E-Jet printing process. It was usually used that the control time less than 0.5 ms can be considered as real-time.^{32,33}

The flow diagram of the control process is shown in Fig. 2. In control of the DoD E-Jet printing process, a signal detector with a

**FIG. 2.** Schematic of the DoD E-jet printing process with current detection and feedback control.

sampling frequency of 30 kHz was used for measuring the current, which took about 60 μ s. Then, the data acquisition (maximum sampling frequency is 250 kHz; maximum throughput is 500 kb s $^{-1}$) was employed to read current data, which took about 25 μ s. These current data, as an input variable of closed-loop feedback control, will be processed by the control algorithm in LabVIEW in which the current scaling law was used as a key controlling equation. Then, the required flow rate will be calculated to match the expected current. Afterward, the controlling coding of the required flow rate was fed to the syringe pump in real-time. The whole controlling period is about 0.35 ms.

In this paper, the measured current data and droplet size were presented as mean \pm standard deviations (SDs). The printing experiments at every printing condition were performed more than three times. In addition, the statistical analysis of the measured current and the corresponding droplet sizes was carried out. Then, the standard deviation of the measurement results was calculated.

III. RESULTS AND DISCUSSION

A. Current characteristic analysis in dripping and microdripping modes

A high speed camera perpendicular to the needle was used to observe the jetting behavior under different printing parameters. As shown in Figs. 3(a) and 3(b), the increase in the applied voltage led to the change from the dripping mode to microripping mode. In the dripping mode [Fig. 3(a)], the pendant droplets dropped off from the needle mainly due to the gravitational force. In the microripping

mode [Fig. 3(b)], the small sized droplet was continuously generated from the hemispherical shape liquid at the needle tip due to the imbalance of the surface tension and the electric tangential force. Figures 3(c)–3(e) show the current characteristics along with the printed structures in dripping and microdripping modes. When the printing was performed in the dripping mode [Fig. 3(c)], the electric force applied on the graphene ink surface was insufficient to form continuous ejection. The discontinuous droplets dropped under the supplement of flow and the force of gravity. It was observed at this situation that the current curve measured was discontinuous [Fig. 3(c)], and the size of printed droplet was not uniform [Fig. 3(f)]. Furthermore, the current peak was different because of the various sized droplets carrying different amount of charges. On the other hand, the current value is zero when no droplet falling down and the current value increases when the droplet size increases. In brief, the current peak signal appeared just with the formation of droplet and the peak value was proportional to the droplet size. In contrast, when the printing was performed at the microdripping mode [Figs. 3(d) and 3(e)], it was indicated that the current curve was continuous and smooth at a certain value when the printing process was stable and the printed droplet size is uniform [Fig. 3(h)]. It was also can be seen that this stable microdripping mode was desirable for the DoD E-Jet printing technique.

B. Current analysis at different printing parameters

The DOD E-Jet printing is a very complicated process because it includes many operating parameters, such as the applied voltage, pulse frequency, flow rate, needle size, needle-substrate distance,

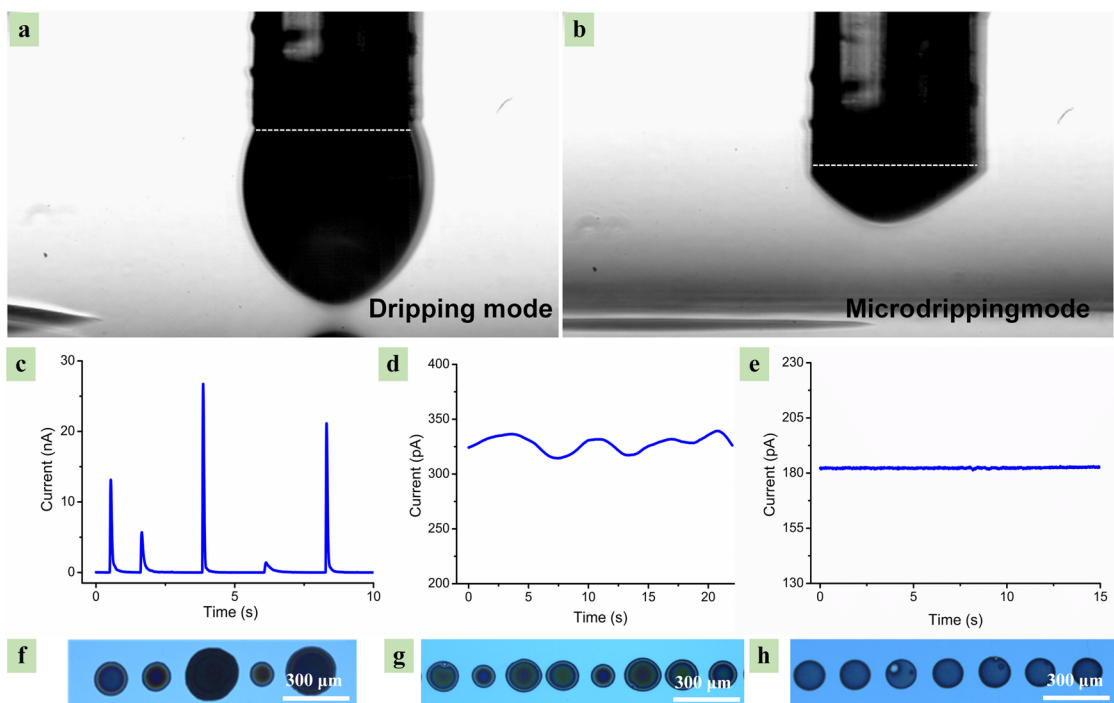


FIG. 3. (a) Printing in the dripping mode, (b) printing in the microdripping mode, (c) current characteristic in the dripping mode, [(d) and (e)] current characteristic in the microdripping mode, (f) printed structure in the dripping mode, and [(g) and (h)] printed structure in the microdripping mode.

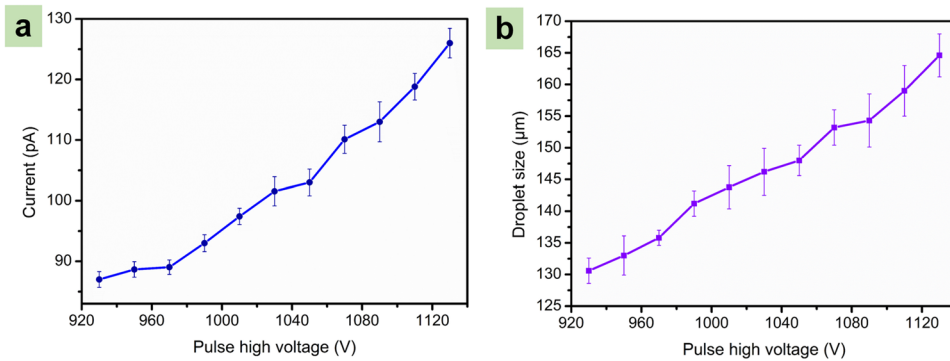


FIG. 4. (a) The relationship between the current and pulse high voltages and (b) the relationship between the droplet size and pulse high voltages.

and ink properties. Moreover, the printing process involves complex dynamics, uncertainties, and external noises. The charges accumulate on the ink surface when a voltage is applied on the needle. Then, the charges move directionally along with the jet and the current is generated as droplets fall on the substrate sequentially. In order to verify the consistency between the measured current and theoretical current, the comparison between these two results was carried out. According to the surface charge density described by Taylor's theory, the corresponding current of the printing ink can be calculated approximately as follows:³⁴

$$I_t = (\gamma Q K / \varepsilon_0)^{1/2}, \quad (1)$$

where γ is the gas-liquid surface tension, Q is the flow rate, K is the electrical conductivity, ε_0 is the vacuum permittivity, and I_t is the current. According to the properties of graphene dispersion and printing parameters (applied voltage of 1000 V, flow rate of $0.02 \mu\text{l min}^{-1}$), the theoretical current of graphene was 94 nA. Compared with the measured current value of 97 ± 2.3 nA [Fig. 4(a)], the theoretical and measured current results were consistent.

The relationship between current, droplet size, and printing parameters were investigated in the stable microdripping printing mode. When the pulse voltage was applied on the ink, the droplet was generated only at the voltage of peak range (pulse high voltage). As shown in Fig. 4, the current characteristic and droplet size were studied at different pulse high voltages, ranging from 930 V to 1130 V. The other printing parameters including the

needle-substrate distance, flow rate, pulse width, low voltage, and pulse frequency were maintained constant at $200 \mu\text{m}$, $0.02 \mu\text{l min}^{-1}$, 10 ms, 680 V, and 5 Hz, respectively. It can be seen that the current and droplet size increased when the applied voltage increased. This is because that the surface charge of every droplet increased with the increase in the applied voltage. As a result, the value of charges increased with the increase in the droplet result in the increase in current. On the other hand, it is easier to overcome the surface tension of the ink and print more droplets under the larger electric field force with the increase in high voltage. At this situation, the size of the printed droplet increased. It was observed during the experiment that when the pulse high voltage was less than 930 V, it was not enough to ensure that the droplet generated from the needle continuously and then the current value was discontinuous. Moreover, when the pulse high voltage was higher than 1200 V, the breakdown between the needle and substrate appeared and the current measurement and control system showed short circuit.

Figure 5 shows the current characteristics and the printed droplet size at different pulse frequencies, ranging from 3 Hz to 11 Hz. In this section, the needle-substrate distance, flow rate, pulse width, low voltage, and pulse high voltage were kept constant at $220 \mu\text{m}$, $0.025 \mu\text{l min}^{-1}$, 1 ms, 700 V, and 1100 V, respectively. It was found that the current was increased as the enhancement of the pulse frequency (Fig. 5). The number of droplets printed per unit time increased when the pulse frequency was increased from 3 Hz to 11 Hz; therefore, droplets falling on the substrate increased, resulting in the increase of the measured current. As shown in Figs. 5(b)–5(f),

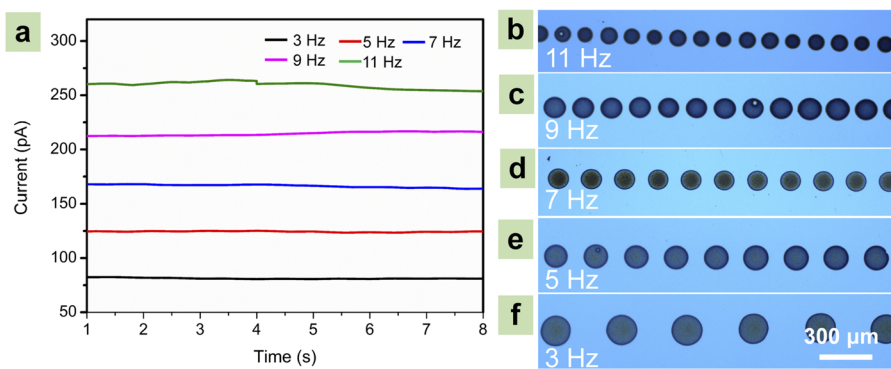


FIG. 5. (a) The relationships between current and frequency and the printed droplet at the frequency of 11 Hz (b), 9 Hz (c), 7 Hz (d), 5 Hz (e), and 3 Hz (f).

when the frequency changed from 3 Hz to 11 Hz, the average size of the printed droplets was $167.6 \pm 1.8 \mu\text{m}$, $135.5 \pm 2.5 \mu\text{m}$, $130.5 \pm 2.4 \mu\text{m}$, $122.2 \pm 2.7 \mu\text{m}$, and $116.7 \pm 3.5 \mu\text{m}$, respectively.

Figure 6 shows the current and printed droplet size at different flow rates of $0.01 \mu\text{l min}^{-1}$, $0.02 \mu\text{l min}^{-1}$, $0.025 \mu\text{l min}^{-1}$, $0.03 \mu\text{l min}^{-1}$, and $0.04 \mu\text{l min}^{-1}$. The other printing parameters, including the needle-substrate distance, pulse width, low voltage, pulse high voltage, and pulse frequency were $220 \mu\text{m}$, 2 ms, 700 V, 1000 V, and 5 Hz, respectively. As shown in **Fig. 6(a)**, it was observed that the current increased with the increase in the flow rate. This is mainly because that when the volume of droplet increased, the amount of charges carried in the printing droplet increased, resulted in the increase in the current. Furthermore, it was found that the flow rate has a distinct effect on the current compared with other printing parameters. As shown in **Figs. 6(b)–6(f)**, when the flow rate was changed from $0.01 \mu\text{l min}^{-1}$ to $0.04 \mu\text{l min}^{-1}$, the average droplet size of printed structures was $142.4 \pm 1.7 \mu\text{m}$, $171.1 \pm 2.1 \mu\text{m}$, $183.1 \pm 2.3 \mu\text{m}$, $198.6 \pm 2.5 \mu\text{m}$, and $225 \pm 2.9 \mu\text{m}$, respectively. There was about $83 \mu\text{m}$ increase in the droplet size when the flow rate increased from $0.01 \mu\text{l min}^{-1}$ to $0.04 \mu\text{l min}^{-1}$.

C. The analysis of current scaling law in microdripping mode

It was found from the above analysis that the flow rate has a major influence on the current in the microdripping mode. In order to obtain the current scaling law in this printing mode, the effect of flow rate on the measured current at different printing conditions of pulse frequency, pulse high voltage, pulse width, and the needle-substrate distance were studied (**Fig. 7**). The printing parameters of **Fig. 7** are shown in **Table II**.

The curves between the current and flow rate show an obvious exponent relationship. Based on the theoretical analysis of Gañán Calvo and Delamora about current scaling, the total emitted current (I) and the jetting diameter (d_j) depend on the liquid properties, including density (ρ), viscosity (μ), electrical conductivity (K), gas-liquid surface tension (γ), and relative permittivity (β) as well as on the injected flow rate (Q), applied voltage (V), vacuum permittivity (ϵ_0), needle inner diameter (d_n), and the distance between the needle and grounded plate (H). If the parameters of ρ , γ , K , and ϵ_0 were chosen as dimensionally independent values, while other parameters were kept fixed, the equations defining the current and flow rate can

be described as follows:

$$I_0 = (\gamma^2 \epsilon_0 / \rho)^{1/2}, \quad (2)$$

$$Q_0 = \gamma \epsilon_0 / \rho K, \quad (3)$$

where γ is the gas-liquid surface tension, ρ is the ink density, ϵ_0 is the vacuum permittivity, K is the electrical conductivity, Q is the flow rate, and I is the current.

It can be seen from **Fig. 7** that the increase in the flow rate leads to the increase in current. This is because that the increase in the flow rate makes more volume of ink jetting from the needle, which carries more charges. According to the current measured and data investigated from **Fig. 7**, there is an exponent relationship between the dimensionless current I/I_0 and the flow rate Q/Q_0 in the micro-dripping mode. The exponential can be calculated from the data in **Fig. 7**, which is 3.34 in this work using the graphene ink. This current scaling law equation provides a basic relationship between the current and flow rate and can be used for the controlling of the DoD E-Jet printing process,

$$I/I_0 = (Q/Q_0)^{3.34}. \quad (4)$$

D. Modification of printing by current optimization

The consistency of the printed structure is important for the DoD E-Jet printing process. The controllable input signal, including the needle-substrate distance, flow rate, pulse high voltage, and pulse frequency have great effect on the consistency of the printed structure. Therefore, it is important to find a convenient method to control the printing process. In order to overcome this problem, this paper proposed a current measurement and control system to modify the printing process in real-time and control the printed droplet size.

As shown in **Fig. 8**, the relationship map between the current and droplet size was analyzed and defined. The printing parameters of **Fig. 8** are shown in **Table II**. The signal of current can be used for controlling the printing process. When the DoD E-Jet printing was conducted at area I (the red area shown in **Fig. 8**), the printing frequency was less than the pulse frequency and the current value was small (<47 pA). Moreover, the size of the printed droplet at this current range was not uniform and the interval between the adjacent droplets was also inconsistent. When the printing was in area II (the

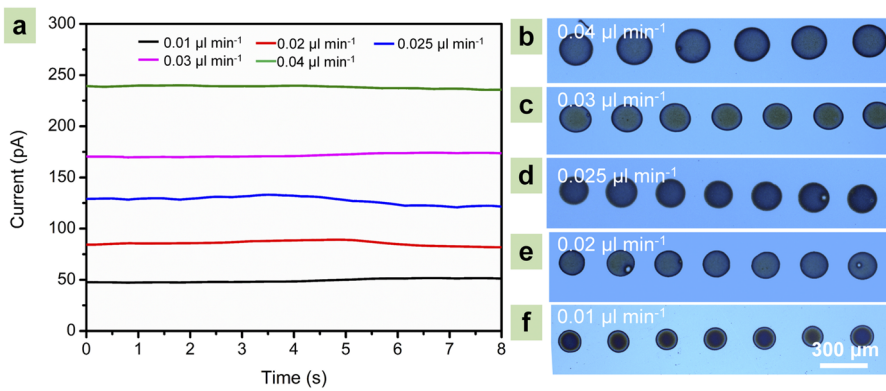


FIG. 6. (a) The relationships between current and flow rate and the printed droplets at the flow rate of $0.04 \mu\text{l min}^{-1}$ (b), $0.03 \mu\text{l min}^{-1}$ (c), $0.025 \mu\text{l min}^{-1}$ (d), $0.02 \mu\text{l min}^{-1}$ (e), and $0.01 \mu\text{l min}^{-1}$ (f).

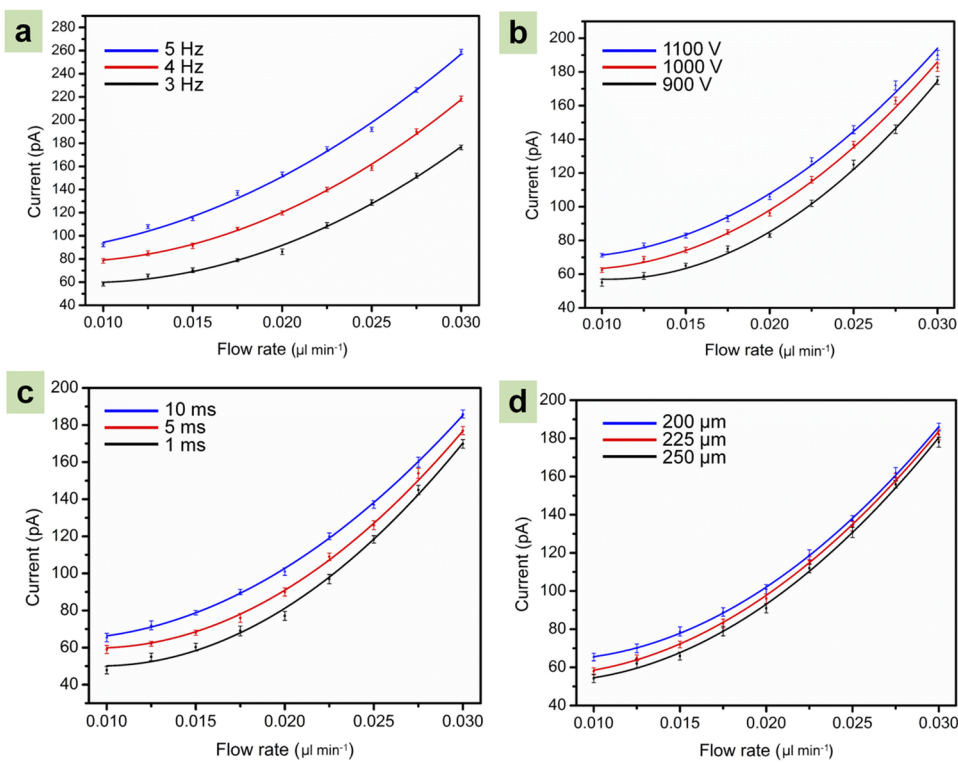


FIG. 7. Curves showing the relationship between current and flow rate in the microdripping mode at different printing parameters: pulse frequency (a), high voltage (b), pulse width (c), and needle-substrate distance (d).

TABLE II. Printing parameters of Figs. 7 and 8.

	High voltage (V)	Low voltage (V)	Flow rate ($\mu\text{l min}^{-1}$)	Needle-substrate distance (μm)	Pulse width (ms)	Frequency (Hz)
Figure 7(a)	900	700	0.025	200	2	3–5
Figure 7(b)	900–1100	700	0.025	200	2	4
Figure 7(c)	1000	700	0.025	200	1, 5, 10	4
Figure 7(d)	1000	700	0.025	200, 225, 250	4	4
Current points in Fig. 8 (pA)						
47.85	1100	700	0.009	220	5	3
86.65	1100	700	0.015	220	5	3
89.53	1050	700	0.016	220	5	3
100.34	1050	700	0.017	220	5	3
111.23	1050	700	0.019	220	5	3
124.82	1050	700	0.022	220	5	3
145.14	1050	700	0.024	220	5	3
163.17	1050	700	0.027	220	3	3
195.24	1050	700	0.032	220	3	3
199.02	1050	700	0.033	220	3	3
211.36	1050	700	0.034	220	3	3
216.7	1050	700	0.035	220	3	3
221.28	1100	700	0.036	220	3	3
239.7	1100	700	0.039	220	3	3
263.93	1100	700	0.042	220	3	3

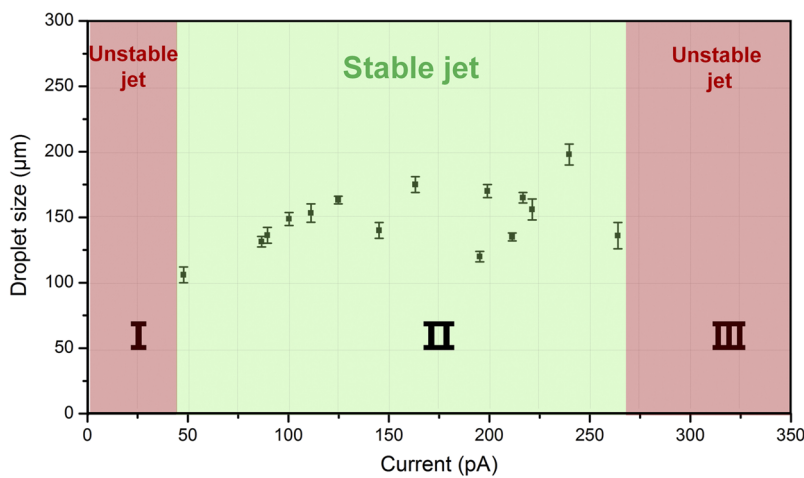


FIG. 8. The map showing the relationship between current, jet stability, and printed droplet size.

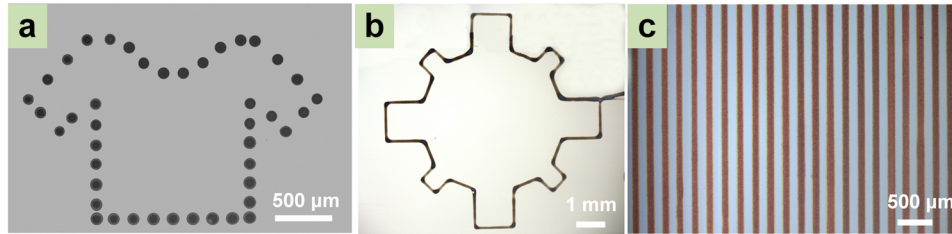


FIG. 9. The printed graphene microstructures: (a) T-shirt, (b) gear, and (c) line array.

green area shown in Fig. 8), the printing frequency was equal to the pulse frequency and the range of the measured current was between 47 pA and 264 pA. The droplet size was smaller and the uniformity of the printed structures increased. However, when the printing was in area III (the red area shown in Fig. 8), the range of measured current was over 264 pA and the deviation of droplet size significantly increased, although the printing frequency was equal to the pulse frequency in this current range.

According to the map showing the stable jet in Fig. 8 (area II), a current value of 80 pA was selected for guiding the printing of graphene microstructures in the microdripping mode. The needle-substrate distance will be slightly different during printing mainly due to the motion error caused by the motion axis and the printing platform. This minor difference can cause the unstable printing process and can be responded by the current. Therefore, the current was controlled in a constant value by fine adjusting the flow rate. For example, the flow rate was adjusted in real-time between 0.016 and $0.019 \mu\text{l min}^{-1}$ to keep current at 80 pA. Graphene patterns of T-shirt, gear, and line array at the typical feature of microscale size were printed on the silicon substrate based on the measured current, which are shown in Figs. 9(a)–9(c). According to the current value (80 pA), the printing parameters of the needle-substrate distance, flow rate, pulse width, low voltage, pulse high voltage, and pulse frequency were kept at 200 μm , $0.016\text{--}0.019 \mu\text{l min}^{-1}$, 1 ms, 680 V, 1000 V, and 5 Hz, respectively. As shown in Fig. 9(a), the droplet diameter of the T-shirt pattern was $110 \pm 5 \mu\text{m}$, which is consistent with the map shown in Fig. 8. During the printing of gear and line array patterns [Figs. 9(b) and 9(c)], the pulse frequency was increased to 50 Hz while other parameters were kept

the same as the printing of the T-shirt pattern. The width of the printed gear and line array was $110 \pm 3 \mu\text{m}$. It can be seen that the printed graphene microstructure presented a uniform feature. The controllable printing of these microscale graphene patterns provides potential applications in electrodes, field transducers, and supercapacitors.

IV. CONCLUSIONS

Drop on demand electrohydrodynamic jet (DoD E-Jet) printing is a promising additive manufacturing technique for M/NEMS devices. The control of parameters during printing is most important for precisely producing micro/nanostructures. In order to maintain the uniform printed droplet size and stable printing status, an instrument of DoD E-Jet printing device equipped with the current measurement and control system was designed and developed. The program for current measurement and control of printing parameters was also realized. The use of this instrument for online monitoring of current and real-time adjusting of the working parameters was aptly demonstrated. Under the condition that the needle size remained unchanged, the effect of the working parameters of voltage, frequency, and flow rate on the current and printing size was discussed, and the current scaling law in the microdripping mode was recognized. Then, the map showing the relationship between the current, droplet size, and printing stability was established. Based on the current measurement and control system and the established relationship, the optimized current and related printing parameters were chosen to print uniform graphene microstructures. This instrument provides an effective method for monitoring,

adjusting, and controlling of the DoD E-Jet printing process, which will be helpful for the improvement of the printed structures and provide a promising manufacturing route for M/NEMS devices.

ACKNOWLEDGMENTS

This research was supported by the National Natural Science Foundation of China (Grant No. 51975104), the National Key R&D Program of China (Grant No. 2018YFA0703200), the Aerospace Science Foundation (Grant No. 2018ZD63004), the Fundamental Research Funds for the Central Universities (Grant No. DUT18LAB17), the State Key Laboratory of Precision Measuring Technology and Instruments (Tianjin University) (Grant No. pilab1804) Science Fund for Creative Research Groups of NSFC (Grant No. 51321004), and the Collaborative Innovation Center of Major Machine Manufacturing in Liaoning.

REFERENCES

- ¹S. V. Murphy and A. Atala, *Nat. Biotechnol.* **32**, 773 (2014).
- ²E. MacDonald and R. Wicker, *Science* **353**, aaf2093 (2016).
- ³K. Fu, Y. Wang, C. Yan, Y. Yao, Y. Chen, J. Dai, S. Lacey, Y. Wang, J. Wan, T. Li, Z. Wang, Y. Xu, and L. Hu, *Adv. Mater.* **28**, 2587 (2016).
- ⁴Z. Yu, Y. Zhao, L. Sun, B. Tian, and Z. Jiang, *Rev. Sci. Instrum.* **84**, 015004 (2013).
- ⁵R. D. Pedde, B. Mirani, A. Navaei, T. Stylian, S. Wong, M. Mehrali, A. Thakur, N. K. Mohtaram, A. Bayati, A. Dolatshahi-Pirouz, M. Nikkhah, S. M. Willerth, and M. Akbari, *Adv. Mater.* **29**, 1606061 (2017).
- ⁶D. Oran, S. G. Rodriguez, R. Gao, S. Asano, M. A. Skylar-Scott, F. Chen, P. W. Tillberg, A. H. Marblestone, and E. S. Boyden, *Science* **362**, 1281 (2018).
- ⁷A. Vyatskikh, S. Delalande, A. Kudo, X. Zhang, C. M. Portela, and J. R. Greer, *Nat. Commun.* **9**, 593 (2018).
- ⁸D. S. Gianola, A. Sedlmayr, R. Moenig, C. A. Volkert, R. C. Major, E. Cyrankowski, S. A. S. Asif, O. L. Warren, and O. Kraft, *Rev. Sci. Instrum.* **82**, 063901 (2011).
- ⁹J. U. Park, M. Hardy, S. J. Kang, K. Barton, K. Adair, D. K. Mukhopadhyay, C. Y. Lee, M. S. Strano, A. G. Alleyne, J. G. Georgiadis, P. M. Ferreira, and J. A. Rogers, *Nat. Mater.* **6**, 782 (2007).
- ¹⁰R. L. Truby and J. A. Lewis, *Nature* **540**, 371 (2016).
- ¹¹Y. Mishnayot, M. Layani, I. Cooperstein, S. Magdassi, and G. Ron, *Rev. Sci. Instrum.* **85**, 085102 (2014).
- ¹²C. H. Kim, J. Jo, and S.-H. Lee, *Rev. Sci. Instrum.* **83**, 065001 (2012).
- ¹³B. H. Kim, M. S. Onses, J. B. Lim, S. Nam, N. Oh, H. Kim, K. J. Yu, J. W. Lee, J. H. Kim, S. K. Kang, C. H. Lee, J. Lee, J. H. Shin, N. H. Kim, C. Leal, M. Shim, and J. A. Rogers, *Nano Lett.* **15**, 969 (2015).
- ¹⁴M. S. Onses, C. Song, L. Williamson, E. Sutanto, P. M. Ferreira, A. G. Alleyne, P. F. Nealey, H. Ahn, and J. A. Rogers, *Nat. Nanotechnol.* **8**, 667 (2013).
- ¹⁵S. Mishra, K. L. Barton, A. G. Alleyne, P. M. Ferreira, and J. A. Rogers, *J. Micromech. Microeng.* **20**, 095026 (2010).
- ¹⁶F. D. Prasetyo, H. T. Yudistira, V. D. Nguyen, and D. Byun, *J. Micromech. Microeng.* **23**, 095028 (2013).
- ¹⁷K. Rahman, K. Ali, N. M. Muhammad, M.-t. Hyun, and K.-h. Choi, *Appl. Phys. A* **111**, 593 (2012).
- ¹⁸K. Barton, S. Mishra, A. Alleyne, P. Ferreira, and J. Rogers, *Control Eng. Pract.* **19**, 1266 (2011).
- ¹⁹M. S. Onses, E. Sutanto, P. M. Ferreira, A. G. Alleyne, and J. A. Rogers, *Small* **11**, 4237 (2015).
- ²⁰Y. Huang, N. Bu, Y. Duan, Y. Pan, H. Liu, Z. Yin, and Y. Xiong, *Nanoscale* **5**, 12007 (2013).
- ²¹H. Dong, W. W. Carr, and J. F. Morris, *Phys. Fluids* **18**, 072102 (2006).
- ²²H. Dong, W. W. Carr, and J. F. Morris, *Rev. Sci. Instrum.* **77**, 085101 (2006).
- ²³J. He, X. Zhao, J. Chang, and D. Li, *Small* **13**, 1702626 (2017).
- ²⁴H. Ding, C. Zhu, L. Tian, C. Liu, G. Fu, L. Shang, and Z. Gu, *ACS Appl. Mater. Interfaces* **9**, 11933 (2017).
- ²⁵D. Wang, L. Wang, J. Liang, and C. Liu, *Rev. Sci. Instrum.* **83**, 095005 (2012).
- ²⁶H. Qin, X. Zhang, R. Singh, Z. Zhang, and Y. Chen, *AIP Conf. Proc.* **2102**, 070008 (2019).
- ²⁷R. Singh, X. Zhang, Y. Chen, J. Zheng, and H. Qin, *Proc. Manuf.* **17**, 45 (2018).
- ²⁸B. T. Lies, C. Yi, E. Spahr, K. Lin, and Q. Hantang, *Proc. Manuf.* **26**, 29 (2018).
- ²⁹N. Trung Kien, N. Vu Dat, B. Seong, H. Nguyen, J. Park, and D. Byun, *J. Aerosol Sci.* **71**, 29 (2014).
- ³⁰J. Zheng, K. Zhang, J. Jiang, X. Wang, W. Li, Y. Liu, J. Liu, and G. Zheng, *AIP Adv.* **8**, 015122 (2018).
- ³¹G. Zheng, W. Xue, H. Chen, L. Sun, J. Jiang, X. Wang, S. Guo, and W. Li, *Micromachines* **10**, 90 (2019).
- ³²H. T. Zhang, G. P. Ren, Y. Wu, H. W. Sun, J. Huang, Z. Yin, and Y. Yuan, *IEEE Trans. Ind. Electron.* **64**, 8686 (2017).
- ³³H. T. Zhang, Q. Wang, Z. Chen, and F. L. Wei, *IEEE Trans. Control Syst. Technol.* **25**, 611 (2017).
- ³⁴J. F. De La Mora and I. G. Loscertales, *J. Fluid Mech.* **260**, 155 (1994).
- ³⁵A. M. Gañán-Calvo, J. Davila, and A. Barrero, *J. Aerosol Sci.* **28**, 249 (1997).